

A New Analysis Method for the Carrying Capacity of Three-Row Roller Slewing Bearing

Peiyu HE*, Yi Ding*, Yun WANG*, Fuzhu LI*, Weili LIU*, Hua WANG**

*School of Mechanical Engineering, Jiangsu University, Zhenjiang, Jiangsu 212013, China, E-mails: hepeiyu@ujs.edu.cn (Corresponding Author); 2498515094@qq.com; Ywang@ujs.edu.cn; FZLi@ujs.edu.cn; WeiliL@ujs.edu.cn

**School of Mechanical and Power Engineering, Nanjing Tech University, Nanjing 211816, China, E-mail: wangh@njtech.edu.cn

crossref <http://dx.doi.org/10.5755/j02.mech.29914>

1. Introduction

The three-row roller slewing bearing is one of the core components of large-scale rotating equipment, which plays a role in relative rotational movement and load transfer. It comprises of inner and outer rings and three rows of rollers with different diameters, as shown in Fig. 1. It is widely used in large and heavy equipment such as the shield machine, the wind turbine, and the crane. The axial load and the overturning moment are mainly carried by the rollers with a larger diameter in the horizontal raceway arrangement, and the rollers mainly carry the radial load with a smaller diameter in the vertical raceway arrangement. The harsh working conditions, heavy load conditions, and substantial structure sizes of the three-row roller slewing bearing require extremely high carrying capacity. The calculation accuracy of the carrying capacity of the three-row roller slewing bearing is not only conducive to the structural optimization of the three-row roller slewing bearing but also conducive to the safety and reliability of the three-row roller slewing bearing structure.

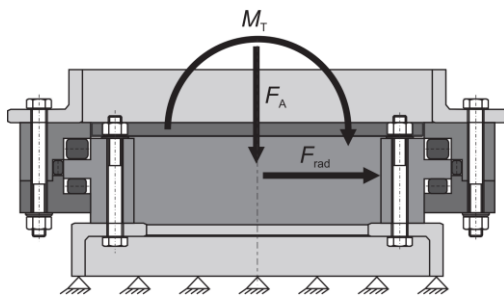


Fig. 1 Structure type of the three-row roller slewing bearing [1]

Hertz contact theory is often used for analytical analysis in the research on the carrying capacity of three-row roller slewing bearings, which studies the local stress distribution and strain distribution of the contact area of two objects. The disadvantage is that it can only solve some simple and uncomplicated contact problems. Much simplification is required before the calculation. The plastic deformation, friction, and heat treatment of the raceway surface at the contact point are not considered [1, 2]. These factors have a significant impact on the carrying capacity of the slewing bearing [3]. Moreover, the Hertz contact theory can only obtain the shape and contact stress of the contact surface between the rolling element and the raceway, and the equivalent stress cannot be obtained. Finite element analysis

can solve the above problems, and the influence of ferrule deformation, upper and lower support structures, and high-strength bolts on the carrying capacity of the three-row roller slewing bearing can also be considered [4].

Finite element models of the carrying capacity analysis of the three-row roller slewing bearing are divided into the solid finite element model and the simplified finite element model. The rings and rollers of the solid finite element model are established as solid models. The three-row roller slewing bearing has a substantial structural size, the number of internal rollers can reach thousands, the contact area between the rollers and the raceway is small, and the contact stress is enormous. The disadvantages of the solid finite element model are that the model is huge, the modeling and calculation time is long, the highly nonlinear analysis requires massive computing equipment, and is prone to non-convergence [5, 6]. The simplified finite element model uses a nonlinear structure to replace the solid roller for the carrying capacity analysis, which significantly simplifies the model scale and effectively improves calculation efficiency. The disadvantages of this method are that it can only obtain the load distribution and the entire circle deformation of the three-row roller slewing bearing and cannot obtain the stress and strain distribution in the contact area between the roller and the raceway [7, 8]. Josu et al use nonlinear structures instead of solid rollers to calculate the carrying capacity to solve these problems, and the maximum contact load obtained is applied to the local contact finite element model to obtain the stress and strain distribution between the roller and the raceway [9]. The local contact finite element model in this method can obtain relatively accurate results by refining the finite element mesh, but the influence of the surrounding raceways cannot be considered. There are errors in the calculation results [10, 11].

The new model of partial rollers and nonlinear springs instead of solid rollers is used to analyze the carrying capacity of the three-row roller slewing bearing in this paper. The new model not only obtains the load distribution, deformation, stress, and strain distribution of the slewing bearing but also reduces the size of the finite element model, avoids the problems of large solid finite element scale and calculation difficulties, and avoids the nonlinear structure replacing the roller finite element model with low calculation accuracy. The new model in this paper provides engineering designers with new methods for analyzing the carrying capacity of three-row roller slewing bearings.

2. Local contact model of three-row roller slewing bearing

2.1. Structure size of the three-row roller slewing bearing

The three-row roller slewing bearing model 130.20.1005 is selected in this paper, and the structural dimensions are shown in Fig. 2. The diameter and length of the upper and lower rollers of the three-row roller slewing bearing are 20 mm, and the number is 120. The center diameter of the upper and lower raceways is 1005 mm. The radial force is not included in the applied load, and the middle row rollers are ignored in the model. According to the carrying capacity of the three-row roller slewing bearing, the axial load is 59,650 N and the overturning moment is 418,000,000 N.mm [12]. The three-row roller slewing bearing uses 42CrMo as the ring material, the elastic model is 21,000 MPa, and the Poisson's ratio is 0.3. The rolling element material is GCr15, the elastic model is 212,000 MPa, and the Poisson's ratio is 0.3 [13].

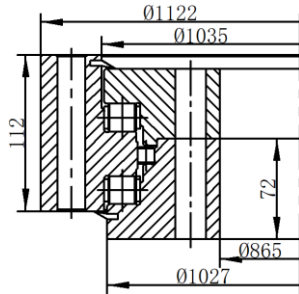


Fig. 2 Dimension of 130.20.1005 model, three-row roller slewing bearing

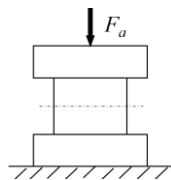


Fig. 3 Schematic diagram of the axial load under individual action

Fig. 3 is a schematic diagram of the contact between the roller and the raceway. When the axial load acts alone, the load of each rolling element is the same, and the external load on the raceway is evenly distributed. Therefore, the contact load between the roller and the raceway is:

$$Q_a = \frac{F_a}{n}, \quad (1)$$

where: F_a is the axial load; Q_a is the contact load under the action of the axial load; n is the roller number.

Fig. 4 is a schematic diagram of the slewing bearing only subject to the overturning moment. The load on the unit arc length at the φ angle is:

$$Q_M = \frac{4M \cos \varphi}{\pi D^2}, \quad (2)$$

where: D is the raceway diameter; M is the overturning moment; Q_M is the maximum contact load under the action of the overturning moment.

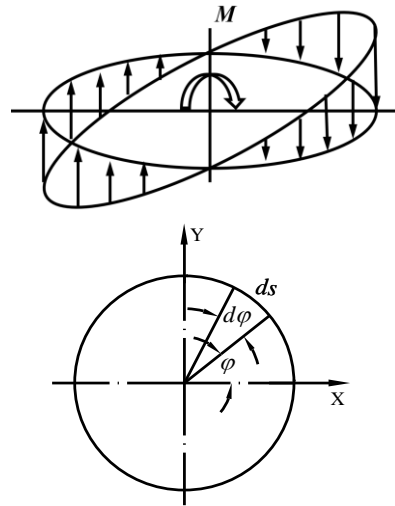


Fig. 4 Schematic diagram of the raceway circumferential pressure distribution

The maximum contact load of the upper row of the three-row roller slewing bearing is obtained by the calculation formula [6]:

$$Q_{max} = Q_{Mmax} + Q_n = \frac{4M}{nD} + \frac{F_a}{n}, \quad (3)$$

where: D is the raceway center diameter; F_a is the axial load; M is the overturning moment; n is the number of rollers; Q is the contact load; Q_a is the contact load under the action of the axial load; Q_M is the contact load under the action of the overturning moment.

2.2. Local finite element model

The new local contact model can obtain the stress and strain distribution of the solid roller finite element model and obtain the load of the simplified finite element model. To verify the new model, the local contact finite element model of the three-row roller slewing bearing for verification and analysis is established in this section. The verified model is used for the overall finite element model analysis of the three-row roller slewing bearing.

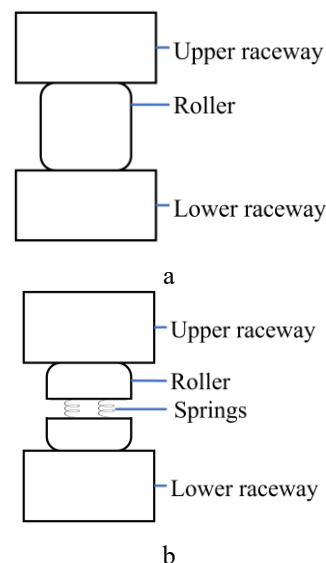


Fig. 5 Local contact finite element of slewing bearing: a) local solid model; b) new model 2; c) model 3

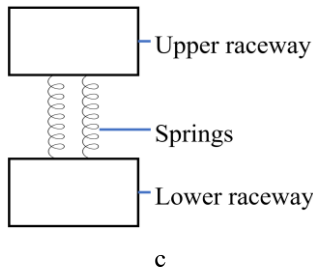


Fig. 5 Continuation

The cylindrical roller chamfer in the local model is 0.7 mm [14]. Model 1 is a finite element model of solid rollers and raceways. Model 2 is a new model of partial contact. Two half rollers and two nonlinear springs are used instead of solid rollers. Both ends of the spring are connected to the end faces of part of the rollers. The assembly of the model is the same as that of model 1. The influence of contact deformation of cylindrical rollers with different diameters is different. To consider the influence of roller diameter on the contact deformation, the load-deformation curve of the roller adopts the following formula [15]:

$$\delta = 4.83 \times 10^{-5} \frac{Q^{0.9}}{l^{0.74}} \left(\frac{1}{D_w} \right)^{0.1}, \quad (4)$$

$$K = \frac{l^{\frac{74}{90}}}{(4.83 \times 10^{-5})^{\frac{10}{9}} \cdot \left(\frac{1}{D_w} \right)^{\frac{1}{9}}}, \quad (5)$$

where: D_w is the roller diameter; K is the spring stiffness; l is the roller length; Q is the contact load; δ is the deformation.

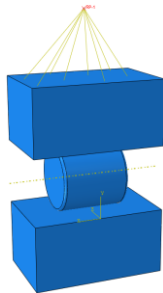


Fig. 6 Local finite element model

The load-deformation curve of the nonlinear spring instead of the solid roller is obtained by Eq. (4). The solid roller is replaced by two nonlinear springs, so the stiffness of a single spring in the model is half the stiffness ($K/2$) in Eq. (5). The local finite element model is shown in Fig. 6. The lower surface of the lower raceway in the three partial models is fully constrained. The reference point RP-1 is set on the upper part of the upper surface of the upper raceway and is coupled with the upper surface. The Y-direction degrees of freedom of the reference point and the roller is released, and the other degrees of freedom are restricted. The load is applied to the reference point. The hexahedral mesh element and the C3D8I element type are selected. The sweep meshing technology and medial axis meshing algorithm are adopted. The roller and the raceway contact pair is

set as surface to surface, the roller is set as the contact main surface, and the raceway is set as the contact slave surface. The friction formula is the Penalty. The friction coefficient is 0.05. The normal behavior is the “Hard contact”.

2.3. Verification of the local model

The overall applied load of the three-row roller slewing bearing is substituted into Eq. (6) to obtain the maximum contact load of the upper row of rollers. To consider the possible error in Eq. 1, loads of 10,000 N, 14,361 N, and 18,722 N are applied to the local contact finite element model. Based on the Hertz contact theory, the maximum contact stress between the roller and the raceway is obtained by Eq. 6 [4]:

$$\sigma_{max} = \sqrt{l\pi \left(\frac{1}{\rho_1} + \frac{1}{\rho_2} \right) \left(\frac{1-u_1^2}{E_1} + \frac{1-u_2^2}{E_2} \right)}, \quad (6)$$

where: E_1 is the elastic modulus of the contact object 1; E_2 is the elastic modulus of the contact object 2; l is the roller length; Q is the contact load; u_1 is the Poisson's ratio of contact object 1; u_2 is the Poisson's ratio of contact object 2; σ_{max} is the maximum contact stress; ρ_1 is the curvature radius 1; ρ_2 is the curvature radius 2.

The distribution of the contact stress of the roller and the raceway surface is roughly the same, and the contact area between the two ends of the roller and the raceway is a high contact stress area, which is caused by the edge effect of the roller, as shown in Fig. 7. When the applied load is 14,361 N, the maximum contact stress of model 1 and model 2 with the maximum contact theoretical error obtained by the Hertz contact theory is 5.97 % and 6.77 %, as shown in Table 1. The error between the new model and the solid roller model is 0.75 % based on the solid roller model, as shown in Table 2. When the load increases to 18,722 N, the error increases. The Hertz contact theory is based on the infinite body and does not consider the plastic deformation and friction of the contact area. Therefore, the applied load increases, and the edge effect of the roller increases. The result of the finite element model is larger than the result of the Hertz contact theory. The above errors are all within the allowable range [16], indicating that the new model has the same effect as the solid roller model in calculating the stress distribution and can be used in the subsequent overall finite element model analysis.

The sum of the loads transmitted by the springs in model 2 and model 3 is the same as the applied load, and the loads transmitted on spring 1 and spring 2 are the same under different loads, as shown in Table 3. This partial model effectively illustrates the feasibility of replacing solid rollers with new models and springs instead of solid rollers in the overall finite element model, which can be used to obtain the load distribution of the entire circle.

Comprehensive analysis shows that the new model 2 can get the same stress and strain distribution as the solid model 1 and can get the load distribution as model 3. The new model 2 has been compared and verified, which can be used in the load capacity analysis of the overall finite element model of three-row roller slewing bearings.

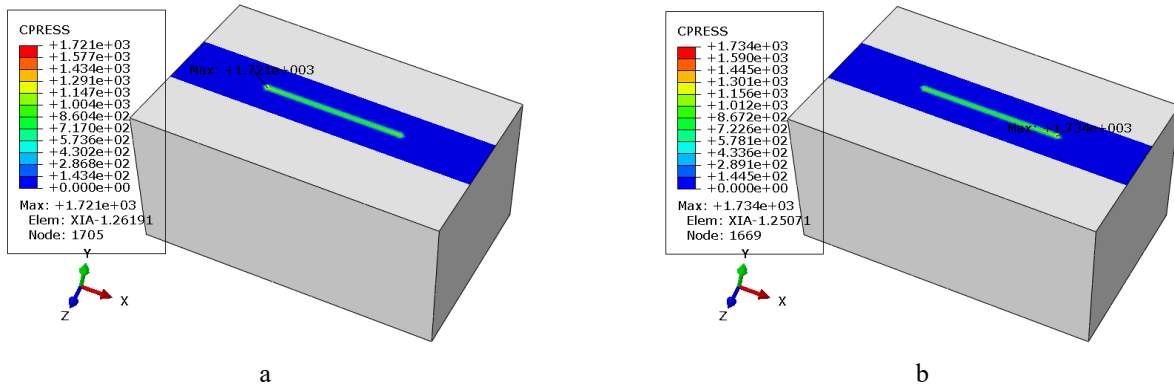


Fig. 7 Contact stress of the raceway with a load of 14,361 N: a) model 1; b) model 2

Table 1

Comparison of contact stress results based on the Hertz contact theory

Load, N		Hertz theory	Model 1	Model 2
10,000	Maximum contact stress, MPa	1,355	1,198	1,207
	Error	Benchmark	11.6%	10.9%
14,361	Maximum contact stress, MPa	1,624	1,721	1,734
	Error	Benchmark	5.97%	6.77%
18,722	Maximum contact stress, MPa	1,855	2,244	2,263
	Error	Benchmark	20.9%	21.9%

Table 2

Comparison of contact stress results based on model 1

Load, N		Model 1	Model 2
10,000	Maximum contact stress, MPa	1,198	1,207
	Error	Benchmark	0.75%
14,361	Maximum contact stress, MPa	1,721	1,734
	Error	Benchmark	0.75%
18,722	Maximum contact stress, MPa)	2,244	2,263
	Error	Benchmark	0.84%

Table 3

Comparison of contact stress results based on model 1

Load, N		Spring 1	Spring 2	Sum	Spring 1	Spring 2	Sum
10,000	Model 2	5,000	5,000	10,000	5,000	5,000	10,000
	Model 3	5,000	5,000	10,000	5,000	5,000	10,000
14,361	Model 2	7,180.5	7,180.5	14,361	7,180.5	7,180.5	14,361
	Model 3	7,180.5	7,180.5	14,361	7,180.5	7,180.5	14,361
18,722	Model 2	9,361	9,361	18,722	9,361	9,361	18,722
	Model 3	9,361	9,361	18,722	9,361	9,361	18,722

3. Overall model of three-row roller slewing bearing

3.1. Overall finite element model

The three-row roller slewing bearing is a large ring structure. To reduce the scale of the calculation model, a half model of the slewing bearing is established. The RP-1 (reference point) is set on the center axis of the three-row roller slewing bearing. The RP-1 is coupled with the upper-end face of the outer ring, and loads and boundary conditions are applied to the RP-1. The Y-axis movement degrees of freedom and Z-axis rotation degrees of freedom of the RP-1 is released, and other degrees of freedom are restricted. The lower surface of the inner raceway is fully constrained. Symmetrical constraints are imposed on the end faces of the inner and outer ring sections. The finite element mesh type of three-row roller slewing bearing is C3D8I and hexagonal mesh [17]. The rollers of the overall model 1 are replaced by two partial rollers and two springs. The rollers of the

overall model 2 are replaced by two springs, as shown in Fig. 8. The load deformation curve of the two springs is half of the roller load deformation curve.

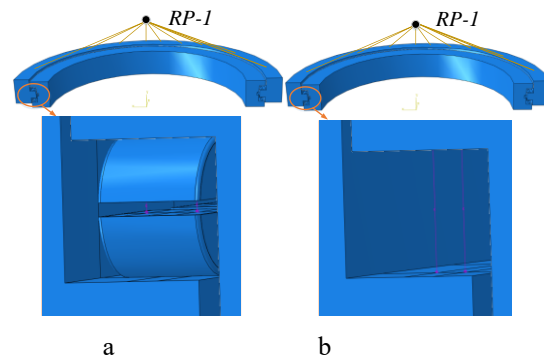


Fig. 8 Overall model: a) model 1; b) model 2

3.2. Test verification of the overall model

The overall test verification of 130.20.1005 type three-row roller slewing bearing is carried out on the slewing bearing test bench. The slewing bearing test bench comprises a loading system, a driving system, and a measurement and control system. Fig. 9 is the structure diagram of the test bench. The axial load and overturning moment are applied by hydraulic cylinders. Strain gauges are installed on the inner circumference of the slewing bearing to obtain the strain of the ring. The location and number of the strain gauges are shown in Fig. 10.

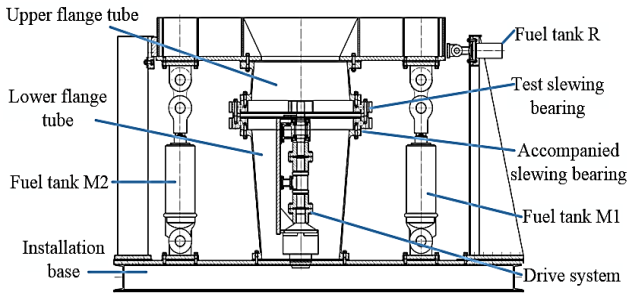


Fig. 9 Schematic diagram of the slewing bearing test stand structure

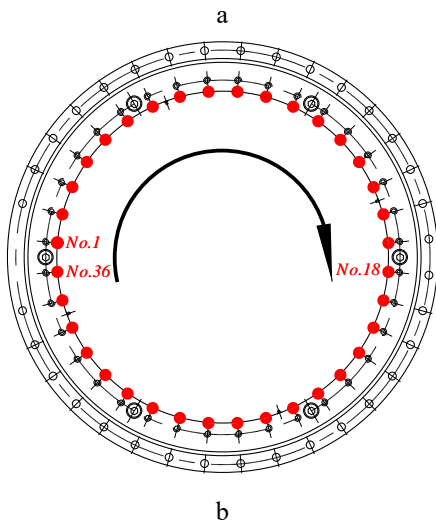


Fig. 10 Three-row roller slewing bearing strain gauge measuring point position layout: a) strain gauge setting; b) strain gauge distribution

The strain at the same position where the new model is attached to the strain gauge is extracted. The test data is averaged after three measurements. The load distribution obtained in the experiment is different from the results of the new model, but the distribution areas of light and

heavy loads and the changing trend of the load distribution are relatively consistent, as shown in Fig. 11, which can prove the reliability of the analysis results of the new model.

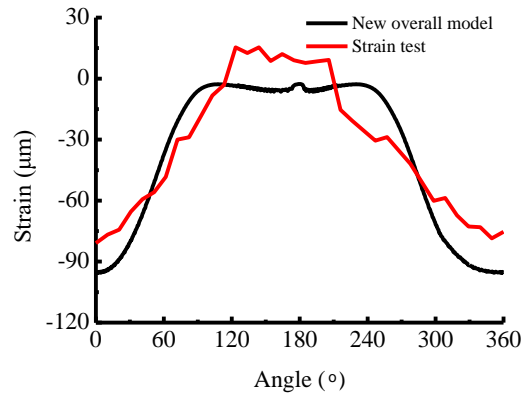


Fig. 11 Comparison of the inner ring strain and test strain of the overall new model

4. Results discussion and analysis

4.1. Discussion and analysis of the overall model

The load distribution trends of the overall model 1 and the overall model 2 are roughly the same. The high load area is slightly different, as shown in Fig. 12. The main reason is that part of the rollers in the overall model 1 are in contact with the raceway. The rollers are in contact with the raceway when loaded. The rollers are separated from the raceway when not loaded. The position of the spring relative to the upper and lower raceways changes. The spring of the overall model 2 is fixed on the upper and lower raceways at both ends during modeling, and the position of the spring relative to the upper and lower raceways is fixed. Comprehensive analysis shows that the overall new model 1 and the overall model 2 have the same effect on obtaining the load distribution of the slewing bearing.

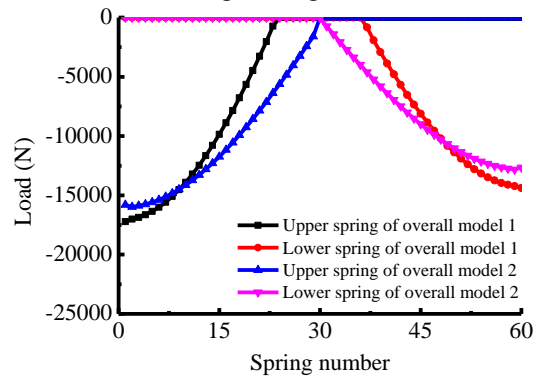


Fig. 12 Comparison of the load distribution between the overall model 1 and the overall model 2

The overall model 1 and the overall model 2 of Fig. 13 have the same deformation distribution under the same load, which shows that model 1 and model 2 have the same effect in analyzing the deformation of the slewing bearing. The entire circle deformation distribution of the overall model 1 and the overall model 2 are consistent, as shown in Fig. 13. The deformation is most significant where the axial load and the overturning moment are superimposed.

4.2. Discussion and analysis of local model

Table 4

The maximum contact load obtained by the finite element model is significantly greater than Eq. (3), as shown in Table 4. The empirical formula is based on the rigid ferrule, which only deforms locally in the contact between the roller and the raceway, and does not consider the influence of the uneven deformation of the ferrule and the supporting structure on the load distribution. The slewing bearing ring and supporting structure are large in size, complicated in load, the ring stiffness is relatively small, and the bending and torsion deformation cannot be ignored. The model based on this assumption has insufficient accuracy in the calculation results in some cases.

Comparison of the maximum contact load in the model with the empirical formula

	Eq. (3)	Overall model 1	Overall model 2
Maximum contact load, N	14,361	17,216	15,807

The high contact stress area of the three-row roller slewing bearing is located at both ends of the direction in which the overturning moment is applied, as shown in Fig. 14. The contact stress distribution of a single roller and race-

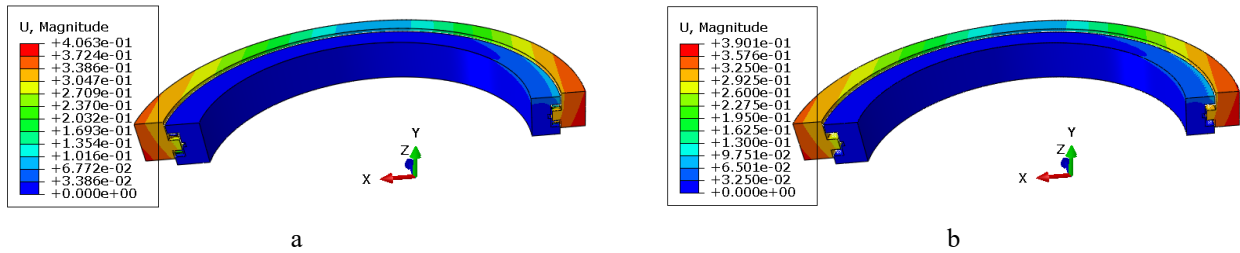


Fig. 13 Deformation comparison: a) the overall model 1; b) the overall model 2

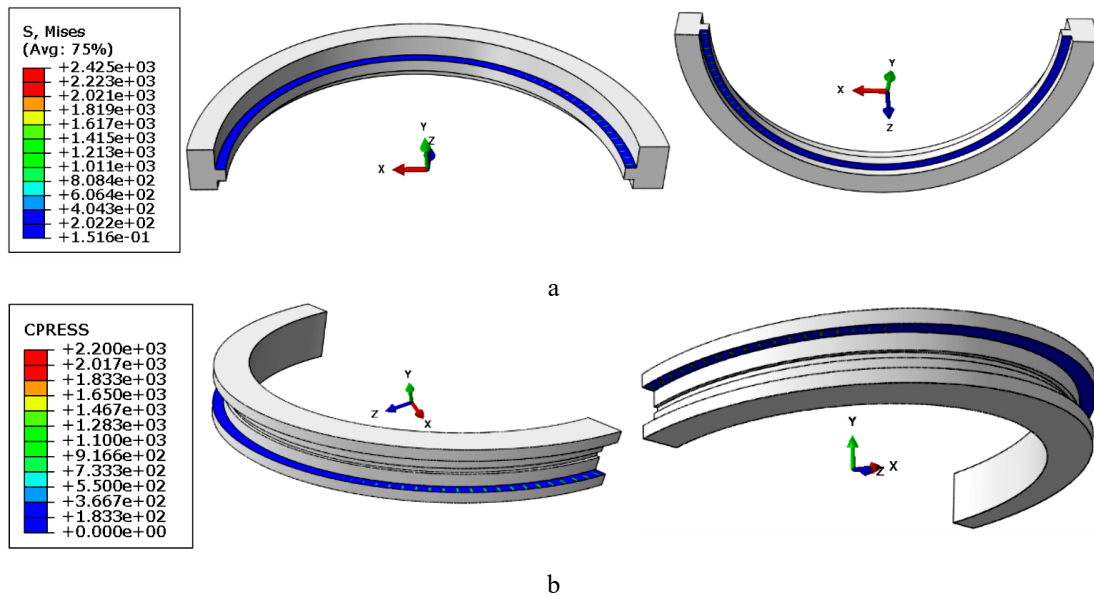


Fig. 14 Contact stress of the new model: a-outer ring, b- inner ring

way is the same as that of the local contact finite element model. The maximum contact stress obtained by the new overall finite element model is greater than the contact stress obtained by bringing the maximum contact load into the local finite element model through the empirical formula, as shown in Fig. 7 and Fig. 14.

5. Conclusions

A new calculation model for the carrying capacity of three-row roller slewing bearing is presented in this paper. The new model obtains the same stress and strain analysis as the solid model and obtains the load distribution and full circle deformation as the simplified model, which improves the efficiency and accuracy of the calculation of the carrying capacity of the three-row roller slewing bearing. The conclusions reached are as follows:

1. The result obtained by the empirical formula for the maximum contact load is less than the result obtained by the overall finite element model. The maximum contact load obtained by the overall finite element model is brought into the local contact finite element, and the maximum contact stress value obtained is less than the maximum contact stress value obtained by the overall finite element model.

2. The maximum contact load obtained by replacing the solid roller finite element model with two nonlinear springs is smaller than the overall finite element model obtained by the new model; the load distribution trend obtained by replacing the solid roller finite element model with two nonlinear springs is consistent with the new model.

The calculation method of carrying capacity of three-row roller slewing bearing proposed in this paper provides a new idea and new method for engineering designers, which has significant practical application value.

Funding

The authors gratefully acknowledge the support provided by the National Natural Science Foundation of China (No. 52105259), Jiangsu Province Key Research and Development Program (BE2016161), and the Jiangsu Postdoctoral Science Foundation (2021K389C).

References

1. **Peter, G.; Miran, U.; Srečko, G.** 2015. Computational assessment of the allowable static contact loading of a roller-slewing bearing's case-hardened raceway, *International Journal of Mechanical Sciences* 94-95: 174-184. <http://dx.doi.org/10.1016/j.ijmecsci.2015.03.006>.
2. **Guanci, C.; Cunzhu, W.; Zhengming, X.** 2016. Effects of supporting structure and bolt connection on the fatigue life and carrying capacity of a slewing bearing, *Proceedings of the Institution of Mechanical Engineers, Part J: Journal of Engineering Tribology* 231(6): 766-782. <http://dx.doi.org/10.1177/1350650116677606>.
3. **Harris, T. A.** 2006. *Rolling bearing analysis*, New York: John Wiley & Sons Inc. p. 121.
4. **Johnson, K. L.** 1985. *Contact mechanics*, Cambridge University Press. p. 90.
5. **Peiyu, H.; Yun, W.** 2020. Effect of high-strength bolts and supporting structures on the carrying capacity of three-row roller slewing bearings, *Proceedings of the Institution of Mechanical Engineers, Part C: Journal of Mechanical Engineering* 235(11): 2053-2064. <http://dx.doi.org/10.1177/0954406220949585>.
6. **Peiyu, H.; Yun, W.; Hong, L.; Erkuo, G.; Hua, W.** 2020. Optimization design of structural parameters of single-row four-point contact ball slewing bearing, *Journal of the Brazilian Society of Mechanical Sciences and Engineering* 42(291): 1-12. <http://dx.doi.org/10.1007/s40430-020-02391-6>.
7. **Peter, G.; Rok, P.; Srečko, G.** 2013. Computational model for determination of static load capacity of three-row roller slewing bearings with arbitrary clearance and predefined raceway deformations, *International Journal of Mechanical Sciences* 73: 82-92. <http://dx.doi.org/10.1016/j.ijmecsci.2013.04.012>.
8. **Peter, G.; Drobne, M.; Srečko, G.** 2013. Computational model for determination of dynamic load capacity of large three-row roller slewing bearing, *Engineering Failure Analysis* 32(9): 44-53. <http://dx.doi.org/10.1016/j.engfailanal.2013.02.030>.
9. **Josu, A.; Mikel, A.; Rafael, A.; Igor, F. B.** 2012. Theoretical calculation of general static load-carrying capacity for the design and selection of three-row roller slewing bearings, *Mechanism and Machine Theory* 48: 52-61. <http://dx.doi.org/10.1016/j.mechmachtheory.2011.09.003>.
10. **Ludwik, K.** 2006. Modelling of rollers in calculation of slewing bearing with the use of finite elements, *Mechanism and Machine Theory* 41(11): 1359-1376. <http://dx.doi.org/10.1016/j.mechmachtheory.2005.12.007>.
11. **Peter, G.; Rok, P.; Srečko, G.** 2010. Load capacity of a three-row roller slewing bearing raceway, *Procedia Engineering* 10: 1196-1201. <http://dx.doi.org/10.1016/j.proeng.2011.04.199>.
12. JB/T 2300-2011. 2011. *Slewing bearing*, In: People's Republic of China Machinery Industry Standards, China.
13. **Iker, H.; Josu, A.; Mikel, A.; Ibai, C.; Iñigo, E.** 2019. Load distribution and friction torque in four-point contact slewing bearings considering manufacturing errors and ring flexibility, *Mechanism and Machine Theory* 137: 23-36. <https://doi.org/10.1016/j.mechmachtheory.2019.03.008>.
14. GB/T 4661-2002. 2002. *Rolling bearings - cylindrical rollers*, In: People's Republic of China Machinery Industry Standards, China.
15. **Jiwei, L.; Tianyu, L.** 2009. *Rolling bearing analysis and calculation*, Beijing: Machinery Industry Press. p. 114.
16. **Jinfeng, C.; Yiping, S.** 2009. *ABAQUS finite element analysis frequently asked questions*, Beijing: Mechanical Industry Press. p. 6.
17. **Rong, L.; Hua, W.; Bitao, P.; Xuehai, G.; Haiyong, Z.** 2018. Load distribution calculation of a four-point-contact slewing bearing and its experimental verification, *Experimental Techniques* 42: 243-252. <http://dx.doi.org/10.1007/s40799-018-0237-2>.

P. Y. He, Y. Ding, Y. Wang, F. Z. Li, W. L. Liu, H. Wang

A NEW ANALYSIS METHOD FOR THE CARRYING CAPACITY OF THREE-ROW ROLLER SLEWING BEARING

Summary

Three-row roller slewing bearings are one of the critical core components of large rotating equipment. Heavy-duty conditions have extremely high requirements for the carrying capacity. The new load capacity analysis method proposed in this paper can effectively improve the accuracy and efficiency of the carrying capacity analysis of three-row roller slewing bearings. The three-row roller slewing bearing solid rollers are replaced in the model by the upper and lower halves of the rollers and two springs. The local contact model of the three-row roller slewing bearing was established and verified by the Hertz contact theory. The overall finite element model of the three-row roller slewing bearing was verified by strain tests. The new method can calculate the stress and strain distribution, load distribution, and deformation of the entire circle of the three-row roller slewing bearing and reduce the mesh number of the finite element of the overall model. Roller chamfer can also be considered closer to the actual working conditions and improves calculation efficiency and accuracy.

Keywords: three-row roller slewing bearing, carrying capacity, load distribution, stress distribution, new finite element model.

Received November 30, 2021

Accepted August 24, 2022

